STARS

University of Central Florida
STARS

Faculty Bibliography 2010s

Faculty Bibliography

1-1-2010

Modeling and simulation of the horizontal component of the geomagnetic field by fractional stochastic differential equations in conjunction with empirical mode decomposition

Zu-Guo Yu

Vo Anh
University of Central Florida

Yang Wang

Dong Mao

James Wanliss

Find similar works at: https://stars.library.ucf.edu/facultybib2010
University of Central Florida Libraries http://library.ucf.edu

Recommended Citation

University of Central Florida

STARS
Showcase of Text, Archives, Research & Scholarship

Modeling and simulation of the horizontal component of the geomagnetic field by fractional stochastic differential equations in conjunction with empirical mode decomposition

Zu-Guo Yu,[1,2] Vo Anh,[1,3] Yang Wang,[4] Dong Mao,[4] and James Wanliss[5]

[1] In this paper, we investigate the characteristics and develop a stochastic model for the horizontal component B_x of the magnetic field at 22 stations of the global near-real-time magnetic observatory network INTERMAGNET. The model is in the form of a fractional stochastic differential equation. A method to estimate the parameters on the basis of observed data and to simulate the data using the model is given. The degree of fractional differentiation and the alpha-stability exponent of the process are employed to cluster the stations. The B_x time series possess pronounced local trends, which must be removed before modeling and simulation can be performed. This trend removal is carried out by an empirical mode decomposition. An outcome is an efficient method to simulate the B_x time series by empirical mode decomposition and fractional stochastic differential equation. The numerical results indicate the existence of two distinct clusters of the INTERMAGNET: one in the mid- and low latitudes consistent with the D_{st} index, and the other above geomagnetic latitude 60°N consistent with the AE index. This clustering corresponds to the inner magnetosphere and the outer magnetosphere, respectively.

1. Introduction

[2] Earlier works by *Consolini et al.* [1996], *Uritsky and Pudovkin* [1998], *Chapman et al.* [1998], and *Chang* [1999] in modeling the magnetosphere in the framework of self-organized criticality (SOC) motivated many recent studies on stochastic properties of the magnetosphere and related geomagnetic indices. In an SOC model, simple local interactions produce complex global signatures of a system. These signatures may appear in the form of power law scaling in the probability distributions or in the power spectra. For example, *Freeman and Watkins* [2002] noted that the probability distribution of the time when the AE index exceeds a given threshold follows a power law distribution. In investigations of the spatial structure of the aurora using ultraviolet images from NASA's POLAR spacecraft, *Lui et al.* [2000] found a power law relationship between the number of bright spots and their area, and

Uritsky et al. [2002] found power laws for the probability distribution of bright spot lifetime and maximum dissipated energy. An explanation of some aspects of these power laws was given by *Klimas et al.* [2004] in an SOC-like reconnection-based model. A review on the scaling in the AE and other geomagnetic indices was provided by *Watkins et al.* [2005].

[3] *Pulkkinen et al.* [2006] developed an Itô-type stochastic model for the AE index to investigate the role of stochastic fluctuations in the global dynamics of the magnetosphere-ionosphere system. *Anh et al.* [2008] provided a fractional stochastic differential equation (FSDE) for the hourly AE index for the period 1978–1987. The memory of the AE time series is represented by a fractional derivative, and its heavy-tailed behavior is modeled by a Lévy noise with inverse Gaussian marginal distribution. The equation has the form of the classical Stokes-Boussinesq-Basset equation of motion for a spherical particle in a fluid with retarded viscosity. The fractional degree of the equation conforms with the previous finding [*Pulkkinen et al.*, 2006] that the fluctuations of the magnetosphere-ionosphere system as seen in the AE reflect the fluctuations in the solar wind: They both possess the same extent of fractional differentiation.

[4] The high-latitude fluctuations, which typically occur above geomagnetic latitude 60°N as manifested in the AE index, reflect solar wind conditions. On the other hand, low-latitude geomagnetic fluctuations, as seen in the D_{st} index, are believed to reflect the inner magnetosphere. *Wanliss and*

[1]Discipline of Mathematical Science, Faculty of Science and Technology, Queensland University of Technology, Brisbane, Australia.
[2]Also at School of Mathematics and Computational Science, Xiangtan University, Hunan, China.
[3]Also at Florida Space Institute, University of Central Florida, Orlando, Florida, USA.
[4]Department of Mathematics, Michigan State University, East Lansing, Michigan, USA.
[5]Presbyterian College, Clinton, South Carolina, USA.

Reynolds [2003] suggested that "examination of low-latitude ground magnetometer signals can provide clues as to whether the magnetosphere is inherently self-organized." *Wanliss and Reynolds* [2003, p. 2025] analyzed hourly magnetometer measurements of total magnetic field strength from six stations at low latitudes over the period 13–18 January 1993. Using spectral analysis and rescaled range analysis, they found, at this hourly resolution, a relative increase of the Hurst exponent with latitude. With regard to the D_{st} itself, *Wanliss* [2004, 2005] and *Wanliss and Dobias* [2007] found that the D_{st} index exhibits a power law spectrum with the Hurst parameter varying over different segments of the time series. This behavior indicates that D_{st} is a multifractional process.

[5] Fractal and multifractal approaches have been quite successful in extracting salient features of physical processes responsible for the near-Earth magnetospheric phenomena [*Lui*, 2002]. Heavy-tailed Lévy-type behavior has been observed in the interplanetary medium and the magnetosphere [*Burlaga*, 1991, 2001; *Burlaga et al.*, 2003; *Kabin and Papitashvili*, 1998; *Lui et al.*, 2000, 2003]. A method to describe the multiple scaling of the measure representation of the D_{st} time series was provided by *Wanliss et al.* [2005]. A prediction method was detailed by *Anh et al.* [2005], together with some numerical results evaluating its performance. A two-dimensional chaos game representation of the D_{st} index and prediction of geomagnetic storm events was proposed by *Yu et al.* [2007]. The spatiotemporal scaling properties of the ground geomagnetic field variations from individual magnetometer stations were studied by *Pulkkinen et al.* [2005] and *Cersosimo and Wanliss* [2007]. *Anh et al.* [2007] used multifractal detrended fluctuation analysis (MF-DFA) to analyze ground magnetic fluctuations for the year 2000. *Yu et al.* [2009] found the storm-flare class dependence through the measure representation [*Yu et al.*, 2001a] and multifractal analysis.

[6] In this paper, we examine ground magnetometer measurements, at high, mid-, and low latitudes, of the horizontal component B_x of the magnetic field. We use the B_x data at 22 stations of the global near-real-time magnetic observatory network INTERMAGNET to classify its different behaviours corresponding to different regions of the magnetosphere.

[7] The Earth's magnetic fluctuations are measured almost continuously by arrays of magnetometers located around the world. The INTERMAGNET program has established a global network of cooperating digital magnetic observatories that currently comprises over 108 observatories. Typical measured parameters include the north (B_x) and east (B_y) components of the horizontal intensity, and the vertical intensity (B_z), or some combination of these. By constantly measuring the magnetic field through programs such as INTERMAGNET, researchers can observe how the field is changing over a period of years and use it to derive a mathematical representation of the Earth's magnetic field and how it is changing. It is noted that the D_{st} is calculated as an hourly average of the horizontal component B_x of the magnetic field at four observatories, namely, Hermanus (33.3° south, 80.3° in magnetic dipole latitude and longitude), Kakioka (26.0° north, 206.0°), Honolulu (21.0° north, 266.4°), and San Juan (29.9° north, 3.2°). These four observatories were chosen because they are close to the magnetic equator and thus are not strongly influenced by auroral current systems. In this paper, we use the horizontal component B_x at 22 stations of INTERMAGNET covering six distinct regions, namely, southwest North America, northeast North America, central Europe, northern Europe, Australasia, and Asia.

[8] The time series of B_x at each station is modeled as the solution of a fractional stochastic differential equation (FSDE) of the form (1) defined in the next section. In this paper, we pay particular attention to the degree of fractional differentiation ν and the α-stability exponent of the noise process $L(t)$ driving equation (1). These two parameters, which express the scaling and fractal behavior of the magnetic field at different locations, can be employed to cluster the stations. We show that the B_x component possesses local trends, which must be removed before the FSDE modeling and simulation can be performed. This trend removal is carried out by an empirical mode decomposition (EMD). The parameter ν is estimated by a detrended fluctuation analysis (DFA), while the parameter α is obtained by fitting the empirical probability density function (PDF) of the data.

[9] The next section details a description of equation (1) and the needed techniques of DFA and EMD. An estimation of equation (1) is then performed for each station. The numerical results are reported in Tables 1 and 2 in section 3 for the cases of raw data without detrending and trend removed, respectively. We show that the estimates of the α-stability exponent are almost similar in both cases and yield consistent clustering. The estimates of the scaling exponent after trend removal supports this clustering. Good simulation of the observed B_x time series is achieved after trend removal. Hence an outcome of the approach of this paper is an efficient method and algorithm for simulation of magnetometer time series by EMD and FSDE. A discussion of the results and some conclusions is given in section 4.

2. Methods

2.1. α-Stable Distribution

[10] The Lévy α-stable distribution is defined by the Fourier transform of its characteristic function [*Nolan*, 2009]

$$f(x; \alpha, \beta, \gamma, \delta) = \int_{-\infty}^{\infty} \varphi(x) e^{-itx} dt,$$

where $\varphi(t)$ is given by

$$\varphi(t) = \exp\{i\delta t - \gamma |t|^{\alpha}[1 + i\beta \, \text{sign}(t) w(t, \alpha)]\},$$

and

$$w(t, \alpha) = \begin{cases} \tan \frac{\alpha\pi}{2}, & \text{if} \quad \alpha \neq 1, \\ \frac{2}{\pi} \log |t|, & \text{if} \quad \alpha = 1, \end{cases}$$

$$\text{sign}(t) = \begin{cases} 1, & \text{if} \quad t > 0, \\ 0, & \text{if} \quad t = 0, \\ -1, & \text{if} \quad t < 0. \end{cases}$$

Here, γ is the scale parameter, α the stability exponent, δ the shift parameter, and β the skewness parameter. The exponent

Table 1. The Estimated Values of the Parameters of the B_x Time Series without Detrending at the Selected Stations[a]

Group	Station	LAT (°)	min(B_x)	max(B_x)	α	β	γ	δ	h
NA1	BOU	48.8	20439	20723	1.5879	−0.8989	13.1886	20648.1	1.1959 ± 0.0334
	FRN	43.7	22767	23174	1.6511	−0.9008	13.6125	23090.4	1.2217 ± 0.0265
	TUC	40.2	24213	24596	1.7114	−0.9900	15.5121	24515.8	1.2492 ± 0.0239
	DLR	38.6	24996	25366	1.7012	−0.9900	15.8343	25288.5	1.2481 ± 0.0294
NA2	FCC	68.3	7388.4	9283.7	1.2705	−0.3183	37.4423	8440.47	1.2188 ± 0.0227
	PBQ	66.8	10022	12144	1.2703	−0.3248	31.9522	11031.1	1.2249 ± 0.0218
	STJ	57.7	17540	18266	1.6525	−0.9253	18.3224	17914.7	1.2192 ± 0.0532
	OTT	56.2	16422	17823	1.6929	−0.8602	18.0112	16967.4	1.1738 ± 0.0723
CEUR	NGK	51.9	18455	18930	1.6334	−0.8597	12.1750	18780.0	1.2998 ± 0.0362
	BDV	48.8	20052	20399	1.5927	−0.8663	11.4755	20296.9	1.3191 ± 0.0300
	FUR	48.3	20608	20939	1.5815	−0.8700	11.2065	20842.9	1.3148 ± 0.0275
	NCK	46.8	20814	21127	1.6256	−0.8641	10.9772	21040.3	1.3010 ± 0.0291
NEUR	ABK	65.9	10189	12258	0.9401	−0.1305	19.9918	11455.2	1.2200 ± 0.0292
	SOD	63.7	10129	12277	0.9829	−0.1366	17.0264	11477.4	1.2122 ± 0.0319
	LOV	57.9	14531	15664	1.6463	−0.4805	12.8191	15297.0	1.2167 ± 0.0664
	NUR	55.1	14041	15352	1.5973	−0.3771	13.1472	14897.1	1.2058 ± 0.0672
AUS	KDU	−22.5	35056	35470	1.7123	−0.3080	16.8851	35357.8	1.4698 ± 0.0468
	CTA	−29.1	31239	31617	1.6017	−0.8537	13.6192	31529.0	1.3500 ± 0.0233
	ASP	−34.2	29665	30014	1.6334	−0.8627	13.6621	29940.2	1.3426 ± 0.0171
ASIA	MMB	34.8	25584	25952	1.6389	−0.9450	14.1416	25877.4	1.2761 ± 0.0367
	BMT	33.9	28170	28528	1.6517	−0.9435	14.2766	28457.1	1.2653 ± 0.0330
	KAK	26.9	29520	29867	1.6464	−0.8909	13.9227	29785.2	1.3146 ± 0.0273

[a]LAT, geomagnetic latitude of the stations.

α controls the kurtosis and lies in the range (0, 2]. The value $\alpha = 2$ corresponds to a Gaussian distribution (for any β), while $\alpha = 1$, $\beta = 0$ corresponds to a Cauchy distribution. The skewness parameter β lies in the range [−1, 1], and when it is zero, the distribution is symmetric and is referred to as a Lévy symmetric α-stable distribution. The scale parameter γ must be larger than 0, and is equal to one half of the variance in the Gaussian case ($\alpha = 2$). The shift δ is a location parameter; it is the mean when $1 < \alpha \leq 2$ and the median when $0 < \alpha < 1$ [*Nikias and Shao*, 1995].

[11] An empirical PDF can be computed from an observed time series. Then maximum likelihood can be used to estimate the parameters α, β, γ, and δ in the α-stable distribution and fit the empirical PDF of the time series.

2.2. Fractional Stochastic Differential Equations Driven by Lévy Noise

[12] *Anh et al.* [2008] provided a description of the non-Gaussianity and possible long-range dependence of the auroral electrojet (*AE*) index in the form of a fractional stochastic differential equation

$$\frac{dX}{dt} + \kappa \mathcal{D}^\nu X(t) = \eta \frac{dL}{dt}, \ \nu \geq 0, \quad (1)$$

where the fractional derivative $\mathcal{D}^\nu$ is defined by [*Podlubny*, 1999, equation (2.138)]

$$\mathcal{D}^\nu \xi(t) = \frac{1}{\Gamma(n-\nu)} \int_0^t (t-\tau)^{n-\nu-1} \frac{d^n \xi(\tau)}{d\tau^n} d\tau, \quad (2)$$

Table 2. The Estimated Values of the Parameters of the Detrended B_x Time Series at the Selected Stations

Group	Station	α	β	γ	δ	h	κ	η	error	RSE e
NA1	BOU	1.5237	−0.8341	9.98987	5.10507	0.8884 ± 0.0321	1.7100	2.2923	0.001800	0.4674
	FRN	1.6169	−0.6796	9.75016	3.42546	0.9423 ± 0.0217	1.4137	2.6347	0.000711	0.3348
	TUC	1.6118	−0.4884	9.31218	2.59578	0.9905 ± 0.0158	1.5345	2.5371	0.001600	0.4885
	DLR	1.5925	−0.4920	9.30300	2.84548	1.0046 ± 0.0159	0.7182	3.8897	0.000590	0.2949
NA2	FCC	1.2604	−0.1740	35.7932	11.1448	0.7891 ± 0.0516	1.4946	1.5746	0.000061	0.4540
	PBQ	1.1022	−0.0650	25.2671	7.05106	0.8242 ± 0.0579	1.5281	1.5281	0.000268	0.8624
	STJ	1.3946	−0.7397	9.76454	6.00033	0.7595 ± 0.0354	1.3055	1.6565	0.000258	0.2902
	OTT	1.3143	−0.7016	10.5020	6.61395	0.7508 ± 0.0325	1.4963	1.6029	0.000352	0.4776
CEUR	NGK	1.5809	−0.6605	9.52715	3.45741	0.8771 ± 0.0376	1.4530	2.5752	0.000385	0.2800
	BDV	1.5513	−0.5706	8.53128	3.08720	0.9432 ± 0.0340	1.2553	2.9598	0.000538	0.2708
	FUR	1.5457	−0.5333	8.24641	2.90425	0.9544 ± 0.0330	1.4121	2.6619	0.000940	0.4166
	NCK	1.5359	−0.5312	7.58381	2.74455	0.9617 ± 0.0313	1.4121	2.6619	0.000940	0.3167
NEUR	ABK	1.0559	−0.0396	25.2279	6.86519	0.7397 ± 0.0496	1.4314	1.5732	0.000066	0.4084
	SOD	1.0434	−0.0085	20.0871	5.14762	0.7340 ± 0.0471	1.3972	1.6238	0.000248	0.7223
	LOV	1.4335	−0.4894	9.81644	3.82705	0.7433 ± 0.0387	1.2118	1.7567	0.000421	0.4593
	NUR	1.3905	−0.3972	10.2271	3.66515	0.7346 ± 0.0385	1.4173	1.7327	0.000791	0.6866
AUS	KDU	1.5580	0.2269	12.9957	−0.77396	1.0145 ± 0.0397	1.4132	2.5488	0.001100	0.5089
	CTA	1.5271	−0.0957	9.43664	1.51390	1.1411 ± 0.0298	1.5722	3.004	0.004200	0.9201
	ASP	1.6202	−0.2351	9.77916	1.85506	1.1191 ± 0.0238	0.6305	4.4862	0.000796	0.3407
ASIA	MMB	1.5712	−0.6727	10.2512	4.06109	0.9737 ± 0.0382	1.2852	2.7394	0.000671	0.3344
	BMT	1.5994	−0.5864	10.1863	3.48716	0.9914 ± 0.0249	1.3488	2.7529	0.000839	0.3680
	KAK	1.6003	−0.3849	9.30575	2.41755	1.0954 ± 0.0273	1.2019	2.7582	0.003200	0.6543

[13] $\nu \in [n-1, n)$, $n = 1, 2, \ldots$, Γ is the gamma function, $\frac{dL}{dt}$ is Lévy noise defined in the distribution sense [see *Mueller*, 1998, for example], and κ, η are constants. Specifically for B_x data, the Lévy noise of equation (1) is assumed to have an α-stable distribution suggested by the form of their empirical PDF. Note that for $\nu = 0$ and $\frac{dL}{dt} = \frac{dW}{dt}$, equation (1) is the classical Langevin equation. If the value of ν is equal to $\frac{1}{2}$, the equation for the time series then takes the form

$$\frac{dX}{dt} + \kappa \mathcal{D}^{\frac{1}{2}} X(t) = \eta \frac{dL}{dt}, \qquad (3)$$

which is the Stokes-Boussinesq-Basset equation in hydrodynamics (driven by Gaussian noise).

[14] An algorithm to get an approximate solution of equation (1) is given in *Anh and McVinish* [2003] and *Anh et al.* [2008]. The algorithm plays an essential role in the estimation of the parameters of the FSDE described below.

[15] A way to simulate random variables from the α-stable distribution is as follows [see *Chambers et al.*, 1976]:

[16] 1. Generate V from a uniform distribution on $[-\pi/2, \pi/2]$ and W from an exponential distribution with mean 1.

[17] 2. For $\alpha \neq 1$, compute

$$X = S_{\alpha,\beta} \frac{\sin[\alpha(V + B_{\alpha,\beta})]}{[\cos(V)]^{1/\alpha}} \left[\frac{\cos[V - \alpha(V + B_{\alpha,\beta})]}{W} \right]^{(1/\alpha - 1)},$$

where

$$B_{\alpha,\beta} = \frac{\arctan\left(\beta \tan \frac{\pi\alpha}{2}\right)}{\alpha},$$

$$S_{\alpha,\beta} = \left[1 + \beta^2 \tan^2\left(\frac{\pi\alpha}{2}\right)\right]^{1/(2\alpha)};$$

for $\alpha = 1$, compute

$$X = \frac{2}{\pi} \left[\left(\frac{\pi}{2} + \beta V\right) \tan V - \beta \ln\left(\frac{\pi W \cos V}{\pi + 2\beta V}\right)\right].$$

Then the stable variable Y can be computed as

$$Y = \begin{cases} \gamma X + \delta, & \text{if } \alpha \neq 1, \\ \gamma X + \frac{2}{\pi} \beta \gamma \ln \gamma + \delta, & \text{if } \alpha = 1, \end{cases}$$

Sample paths of the corresponding Lévy motion can then be generated as

$$L(nh) = \sum_{i=1}^{n} h^{1/\alpha} Y_i, \qquad (4)$$

where the Y_i have an α-stable distribution. This algorithm is needed in the simulation of paths of equation (1).

2.3. Detrended Fluctuation Analysis

[18] To estimate the degree of the fractional derivative, we performed a detrended fluctuation analysis (DFA) [*Peng et al.*, 1994; *Yu et al.*, 2001b, 2006, 2009] of the time series. The DFA is the special case when $q = 2$ of the multifractal detrended fluctuation analysis (MF-DFA) detailed in *Kantelhardt et al.* [2002]. We adopt the algorithm in *Kantelhardt et al.* [2002] and *Movahed et al.* [2006] to

estimate the exponent of DFA in this paper. The procedure consists of five steps. Let $\{X_k\}_{k=1}^{N}$ be a time series of length N.

[19] *Step* 1. The time series is integrated as $Y(i) = \sum_{k=1}^{i} [X_k - X_{ave}]$, $i = 1, 2, \ldots, N$, where X_{ave} is the sample mean over the whole time period.

[20] *Step* 2. The integrated time series is divided into $N_s = [N/s]$ nonoverlapping segments of equal length s. Here, $[N/s]$ is the integer part of N/s. Since the length N of the series is often not a multiple of time scale s, a short part of length $l_e = N - N_s s$ at the end of $Y(i)$ may remain. In order not to disregard this part, the same procedure is repeated starting from the opposite end. Thereby, $2N_s$ segments are obtained altogether.

[21] *Step* 3. Calculate the local trend for each of the $2N_s$ segments by a least-squares fit of the series, then determine the variance

$$F^2(s, \nu) = \frac{1}{s} \sum_{i=1}^{s} \{Y[(\nu - 1)s + i] - y_\nu(i)\}^2, \qquad (5)$$

for each segment $\nu = 1, 2, \ldots, N_s$, and

$$F^2(s, \nu) = \frac{1}{s} \sum_{i=1}^{s} \{Y[(\nu - N_s - 1)s + i + l_e] - y_\nu(i)\}^2, \qquad (6)$$

for each segment $\nu = N_s + 1, N_s + 2, \ldots, 2N_s$. Here $l_e = N - N_s s$, and $y_\nu(i)$ is the first-order polynomial fitting in the νth segment.

[22] *Step* 4. Average over all segments to get the second-order fluctuation function

$$F(s) = \left\{ \frac{1}{2N_s} \sum_{\nu=1}^{2N_s} [F^2(s, \nu)] \right\}^{1/2}. \qquad (7)$$

By construction, $F(s)$ is only defined for $s \geq 3$.

[23] *Step* 5. Determine the scaling behavior of the fluctuation function by analyzing the log-log plots of $F(s)$ versus s, i.e., the power law

$$F(s) \propto s^h, \qquad (8)$$

in some range of time scale s.

[24] *Kantelhardt et al.* [2002] pointed out that for stationary time series, the exponent h for small time scales is identical to the well-known Hurst exponent H; for nonstationary signals, the relation between the exponent h for small scales and the Hurst exponent H is $H = h - 1$. It is well known that for uncorrelated series, the scaling exponent H equals 0.5; the range $0.5 < H < 1$ indicates long memory or persistence; and the range $0 < H < 0.5$ indicates short memory or antipersistence. Hence we can use the value of H calculated from h to detect the nature of memory in time series.

[25] When equation (1) has a stationary solution, *Anh et al.* [2008] suggested a method to estimate the fractional order ν on the basis of an estimation of the scaling exponent h, namely, by the relationship $\nu = h - \frac{1}{2}$.

2.4. Algorithm for Simulation of Fractional Stochastic Differential Equation

[26] First, the empirical PDF of the given time series is computed. We denote this empirical PDF as $f_0(x)$. The

parameters α, β, γ, and δ of the α-stable distribution are then estimated by maximum likelihood. Then we use the DFA to estimate the parameter h and get an estimate for the parameter ν by the relationship $\nu = h - 1/2$. Setting initial values for κ and η, we then generate a sample path of the process $X(t)$ by the approximation algorithm given in *Anh and McVinish* [2003] or *Anh et al.* [2008] on the basis of these estimated values for α, β, γ, δ, and ν in the FSDE (1). Another empirical PDF based on this path of $X(t)$ is then computed.

[27] The procedure is continued for different sets of values of the parameters (κ, η), and we denote the resulting empirical PDF in each iteration as $\widehat{f}(x)$. The estimates of the parameters of equation (1) are those corresponding to

$$\min_{\kappa, \eta} \sum_{i=1}^{N} \left(f_0(x_i) - \widehat{f}(x_i) \right)^2, \qquad (9)$$

where N is the number of points on the PDF curve we selected.

[28] We solve problem (9) by using the function *fminsearch* in MATLAB version 7.1. This algorithm finds the minimum of a scalar function of several variables based on the Nelder-Mead simplex search method [*Lagarias et al.*, 1998]. It should be noted that for each initial set of parameters, the PDF $\widehat{f}(x)$ may have to be computed a large number of times before the minimum is reached.

[29] A solution path of equation (1) on the basis of these estimates is generated. To compare the patterns of the original and simulated series, we replaced values higher than the maximum value or less than the minimum value of the original time series by a uniformly random number between the minimum value and the maximum value.

2.5. Empirical Mode Decomposition

[30] *Lin et al.* [2009] described the traditional *empirical mode decomposition* (EMD) and presented a new approach to EMD. We outline the method of *Lin et al.* [2009] here. The traditional EMD for data, which is a highly adaptive scheme serving as a complement to Fourier and wavelet transforms, was originally proposed by *Huang et al.* [1998]. In EMD, a complicated data set is decomposed into a finite, often small, number of components called *intrinisc mode functions*. EMD has been used successfully in many applications in analyzing a diverse range of data sets in biological and medical sciences, geology, astronomy, engineering, and other fields [e.g., *Janosi and Muller*, 2005; *Shi et al.*, 2008].

[31] The original EMD is obtained through a sifting algorithm: Let $\{t_j\}$ be the local maxima of a signal $X(t)$. The cubic spline $E_U(t)$ connecting the points $\{(t_j, X(t_j))\}$ is referred to as the *upper envelope* of X. The *lower envelope* $E_L(t)$ is similarly obtained from the local minima $\{s_j\}$ of $X(t)$. Then we define the operator $\mathcal{S}$ by

$$\mathcal{S}(X) = X - \frac{1}{2}(E_U + E_L).$$

In the so-called *sifting algorithm*, the first intrinisc mode function the EMD is given by

$$I_1 = \lim_{n \to \infty} \mathcal{S}^n(X).$$

Subsequent intrinisc mode functions in the EMD are obtained recursively by

$$I_k = \lim_{n \to \infty} \mathcal{S}^n(X - I_1 - \ldots - I_{k-1}).$$

The process stops when $Y = X - I_1 - I_2 - \ldots - I_m$ has at most one local maximum or local minimum. This function $Y(t)$ denotes the local trend in $X(t)$.

[32] *Lin et al.* [2009] proposed a new algorithm called *iterative filtering* for EMD. Instead of using the envelopes generated by spline in the sifting algorithm, in this new algorithm a low-pass filter is used to generate a moving average to replace the mean of the envelopes. The essence of the sifting algorithm remains. Let $\mathcal{L}$ be an operator that is a low-pass filter, for which $\mathcal{S}(X)(t)$ represents the moving average of X. We now define

$$\mathcal{T}(X) = X - \mathcal{L}(X).$$

In this approach, the low-pass filter $\mathcal{L}$ is dependent on the data X. For a given $X(t)$, we choose a low-pass filter $\mathcal{L}_1$ accordingly and set $\mathcal{T}_1 = I - \mathcal{L}_1$, where I is the identity operator. The first intrinisc mode function in the new EMD is given by $\lim_{n \to \infty} \mathcal{T}_1^n(X)$, and subsequently the kth intrinisc mode function I_k is obtained first by selecting a low-pass filter $\mathcal{L}_k$ according to the data $X - I_1 - \ldots - I_{k-1}$ and iterations $I_k = \lim_{n \to \infty} \mathcal{T}_k^n(X - I_1 - \ldots - I_{k-1})$, where $\mathcal{T}_k = I - \mathcal{L}_k$. Again, the process stops when $Y = X - I_1 - \ldots - I_m$ has at most one local maximum or local minimum. *Lin et al.* [2009] suggested using the filter $Y = \mathcal{L}(X)$ having the form $Y(n) = \sum_{j=-m}^{m} a_j X(n + j)$ and proved the convergence of the sifting algorithm for a class of filters. We choose the filter given by $a_j = \frac{m - |j| + 1}{m + 1}$, $j = -m, \ldots, m$ for this study, which is simple but works well and is shown to converge [*Lin et al.*, 2009].

3. Data Analysis

[33] We use the above methods to model the hourly averaged time series B_x from 22 INTERMAGNET stations. We collect the stations into six groups for the year 2000: southwest North America (NA1), northeast North America (NA2), central Europe (CEUR), northern Europe (NEUR), Australasia (AUS), and Asia (ASIA). The NA1 group includes the stations Boulder (BOU), Fresno (FRN), Tucson (TUC), and Del Rio (DLR). The NA2 group includes the stations Fort Churchill (FCC), Poste-de-la-Baleine (PBQ), St. John's (STJ), and Ottawa (OTT). The CEUR group includes the stations Niemegk (NGK), Budkov (BDV), Furstenfeldbruck (FUR), and Nagycenk (NCK). The NEUR group includes the stations Abisko (ABK), Sodankyla (SOD), Nurmijarvi (NUR), and Lovo (LOV). The AUS group includes the stations Kakadu (KDU), Charters Towers (CTA), and Alice Springs (ASP). The ASIA group includes the stations Memambetsu (MMB), Beijing Ming Tombs (BMT), and Kakioka (KAK). The geomagnetic latitudes of the stations are listed in Table 1. The top of Figure 1 shows the time series from the BOU station in NA1 as an example.

[34] The empirical density of this time series, as shown in Figure 2, is consistent with a skewed α-stable distribution. Hence we used maximum likelihood (implemented by the program STABLE downloaded from J. P. Nolan's web site:
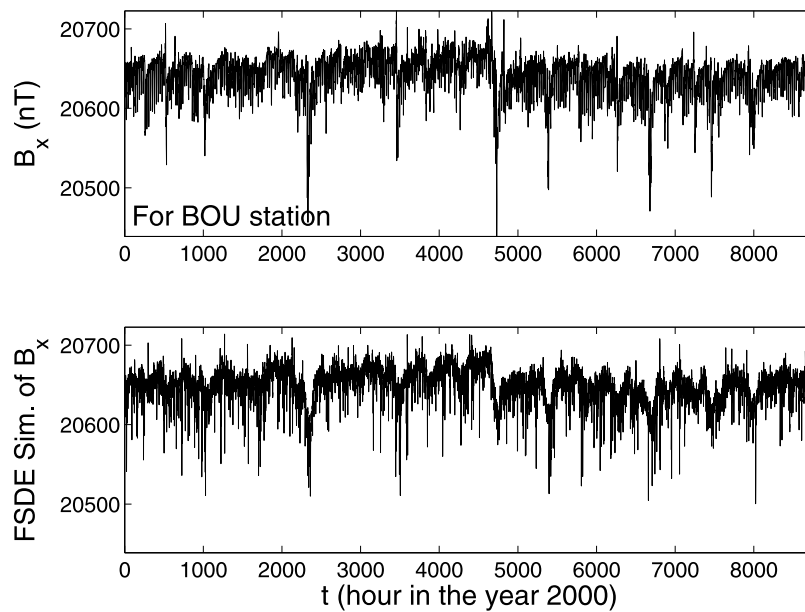
Figure 1. The hourly B_x component of the magnetic field for the year 2000 at station Boulder (BOU) and its fractional stochastic differential equation simulation.

http://www.academic2.american.edu/jpnolan) to estimate the parameters α, β, γ, and δ in the α-stable distribution and generate the corresponding PDF to fit the empirical density of the observed time series. We found that the α-stable distribution provides a reasonably good fit to the probability density of B_x data (see Figure 2). The estimated values of α, β, γ, and δ for B_x of these stations are given in Table 1.

[35] Then we performed a DFA on the B_x data. For the given time series, we found good linear relationships of $\log_{10} F(s)$ versus $\log_{10} s$ in the time scale range of $5 \leq s \leq 25$ hours (almost a day). The estimated values of the expo-

nent h for B_x are given in Table 1. As an example, the DFA slope estimation for the B_x at the BOU station is given in Figure 3. The h values of the B_x time series, which vary in the range $1.0 < h < 1.5$, indicate that the observed B_x time series are nonstationary. From the relationship $H = h - 1$ between the exponent h and the Hurst exponent H for the nonstationary case, the H values varying in the range $0 < H < 0.5$ indicate that the observed B_x time series are antipersistent.

[36] Since the local trends are pronounced in the magnetic field data, we used the traditional EMD [*Huang et al.*, 1998] and the new EMD developed by *Lin et al.* [2009] to get
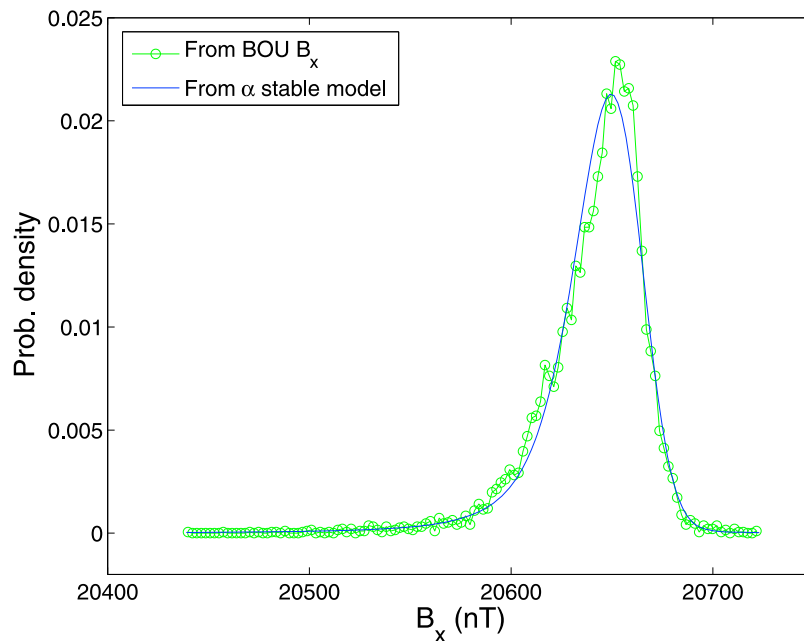
Figure 2. The α-stable fit for the probability density of the hourly component B_x at station Boulder (BOU).
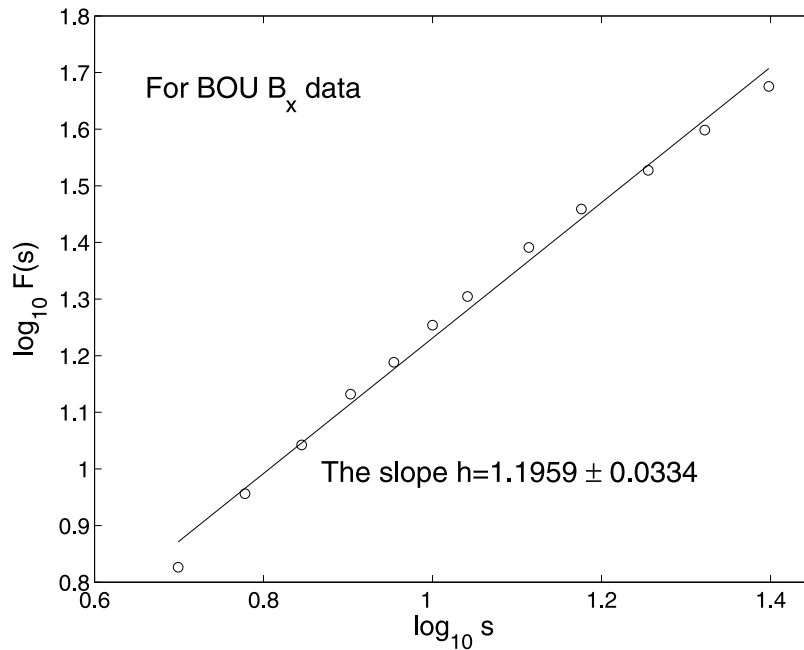
Figure 3. Estimation of the h exponent via the slope of the regression $log_{10}(F(s))$ vs. $log_{10}(s)$ for the B_x time series at station Boulder (BOU) using detrended fluctuation analysis. The slope is the same as h in Table 1.

these local trends. We found that both EMDs can trace out the trends, but the new EMD works slightly better. Hence we only show the results using the new EMD in the following. We used the new EMD to get the intrinisc mode functions as displayed in Figure 4, which show that the randomness becomes less from I_1 to I_4, and I_4 is relatively smooth. Hence we define the local trend of the magnetic field data as $Y = X - (I_1 + I_2 + I_3 + I_4)$ as in *Shi et al.* [2008].

We then removed the local trend from the raw data by $X–Y$ to get the detrended data $(I_1 + I_2 + I_3 + I_4)$, which appear to be stationary. As an example, we get the local trend of B_x data at the BOU station from the bottom of Figure 4 and show the detrended data in the top left column of Figure 5.

[37] We used the fractional FSDE (1) to simulate the detrended data $(I_1 + I_2 + I_3 + I_4)$. The first step is to fit the empirical density of the detrended data using an α-stable
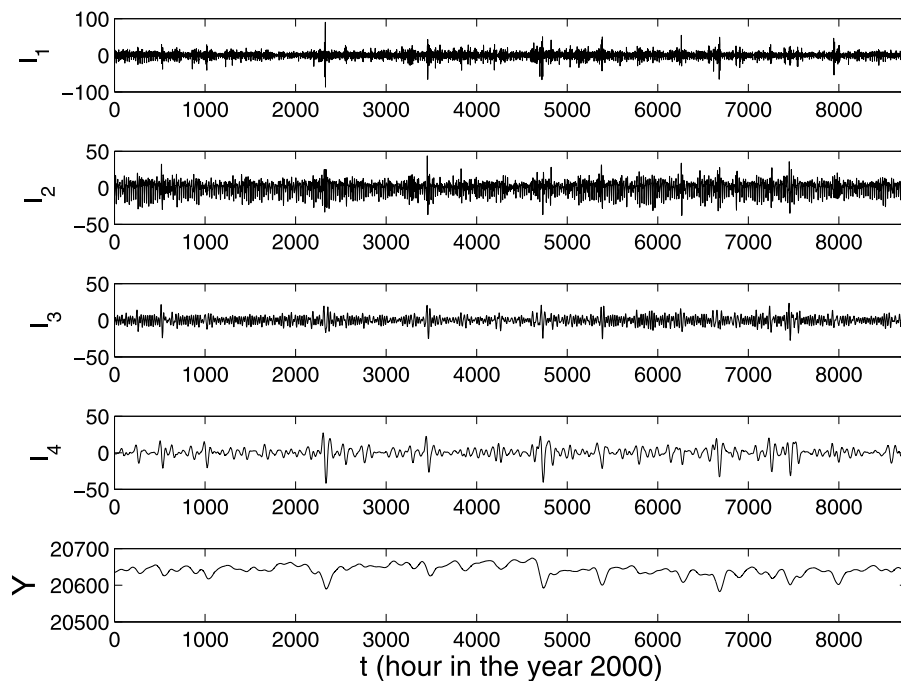
Figure 4. The intrinisc mode functions and trend of the B_x data of station Boulder (BOU) using empirical mode decomposition.
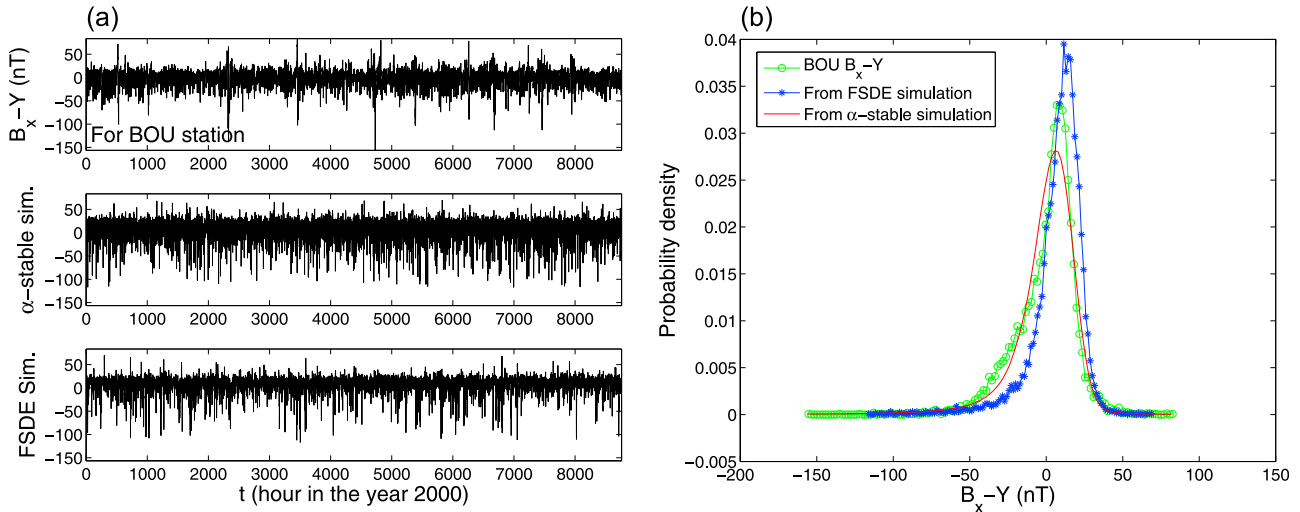
Figure 5. (Left): the fractional stochastic differential equation simulation of the detrended data $B_x - Y$ at station Boulder (BOU). (Right): the corresponding probability density of the detrended data.

distribution. Then we used the slope of DFA in the time scale range $11 \leq s \leq 47$, which gives good linear relationships, to infer the exponent h and get an estimate of the parameter ν by the relationship $\nu = h - 1/2$. Last we fixed the estimated values of the parameters α, β, γ, δ, and ν in the FSDE (1) and used the simulation algorithm given in *Anh et al.* [2008] to estimate the coefficients κ and η by equation (9). In the last step, we set the initial value of (κ, η) as (1.5,1.5) for the NA2 and NEUR stations, and (1.5,2.5) for the other stations, respectively, and set $N = 130$ in equation (9) (one can set the value of N as large as possible; usually a number larger than 100 is sufficient). We found that the FSDE simulates well all detrended B_x time series. As an example, we show the simulation of the detrended B_x time series at the BOU station in the left column of Figure 5 and the corresponding empirical density of the detrended data in its right column. The estimated values of all the parameters α, β, γ, and δ, ν, κ, and η with the error (i.e., the

minimum value in equation (9)) for the detrended B_x at the selected stations are listed in Table 2. Since the statistical estimation of each FSDE is obtained via minimizing the mean square error between the empirical PDEs of the data and simulated paths as defined in equation (9), we evaluate its performance on the basis of the *relative standard error* (RSE) e defined as e_1/e_2, where

$$e_1 = \sqrt{\frac{1}{N} \sum_{i=1}^{N} \left(f(x_i) - \widehat{f}(x_i) \right)^2},$$

$$e_2 = \sqrt{\frac{1}{N} \sum_{i=1}^{N} \left(f(x_i) - f_{ave} \right)^2}.$$

Here, $f(x)$ is the empirical PDF of the detrended data, with average value f_{ave}, and $\widehat{f}(x)$ is the PDF of a simulated path. The goodness of fit is indicated by the result $e < 1.0$ as pointed out by *Anh et al.* [2002a]. The values of the RSE e
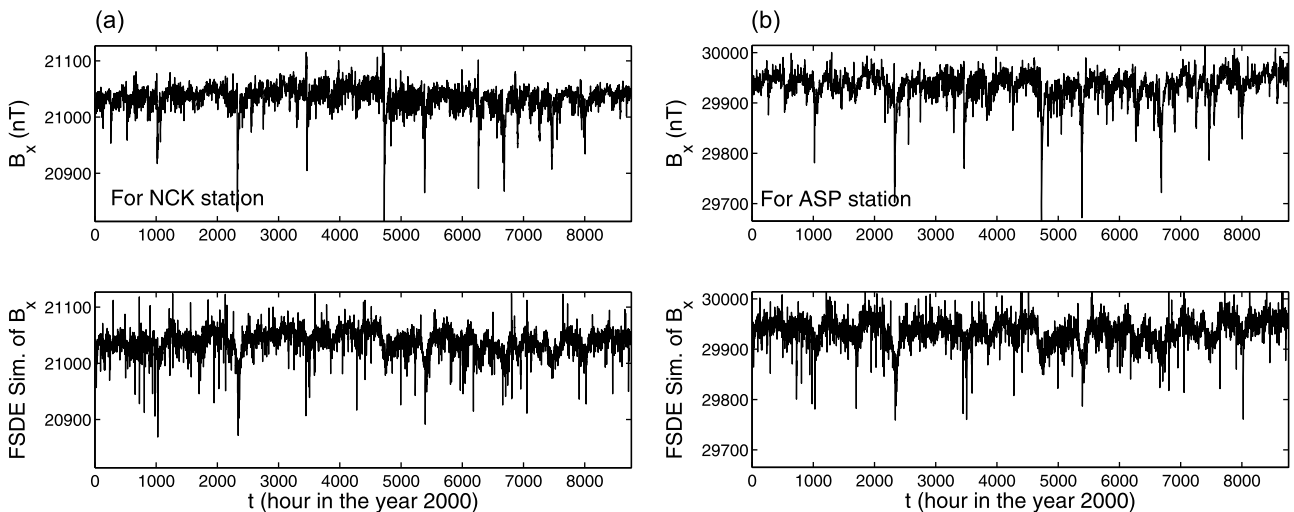
Figure 6. The hourly B_x component for the year 2000 at station Nagycenk (NCK) and its fractional stochastic differential equation simulation (Left), and those at station Alice Springs (ASP) (Right).

for the detrended B_x at the selected stations are listed in Table 2. All the values of e are smaller than 1.0 in Table 2, and most are smaller than 0.5, indicating that the FSDE performs well in simulating detrended data.

[38] If the FSDE simulation of the detrended data is denoted as $\hat{X}_{detrend}$, a simulation of each time series B_x is then obtained as the sum of such a simulated path $\hat{X}_{detrend}$ and the fitted trend Y. As examples, we show the simulation of the B_x time series at the BOU station at the bottom of Figure 1 and the simulations of B_x time series at stations NCK and ASP in Figure 6. The simulated paths trace very well those of the observed time series. The results indicate that the FSDE (1) in combination with EMD provides a good method to model the B_x component of the magnetic field. In fact, we also tried the method on the B_y and B_z components, and the simulations are also excellent for all 22 stations.

[39] A similar FSDE was considered by *Anh et al.* [2008] to model the *AE* index data. The difference between the FSDE in this paper and that used by *Anh et al.* [2008] is the Lévy noise term. The FSDE used by *Anh et al.* [2008] is driven by an inverse Gaussian marginal distribution, whereas the FSDE in this paper is driven by an α-stable distribution. This difference in the selection simply reflects the form of the empirical density in each case. Another difference is that the method used by *Anh et al.* [2008] uses FSDE alone, while we use FSDE and EMD together here. We also tried to simulate the B_x data using the method used by *Anh et al.* [2008], but the simulation results are inadequate. This indicates that the B_x time series are more complicated than the *AE* index.

4. Discussion

[40] The 22 stations as listed in Table 1 together with their geomagnetic latitudes represent the low-latitude stations (the group AUS), the midlatitude stations (the groups NA1, CEUR, ASIA, and the stations STJ and OTT in NA2 and LOV and NUR in NEUR) and those above 60°N (the stations FCC and PBQ in NA2 and ABK and SOD in NEUR). For the purpose of clustering of these stations, the two most significant parameters are the stability exponent α and the degree of differentiation ν (or h as reported). When the time series is stationary, the value ν in the interval (0,1/2) signifies its long-range dependence [*Anh et al.*, 2002b]. When ν tends to 1/2, the time series approaches nonstationarity. On the other hand, it was shown by *Jaffard* [1999] that an α-stable process has multifractal paths; but this multifractality is characterized by a linear singularity spectrum, whereas a typical multifractal process in turbulence has a nonlinear (concave) singularity spectrum.

[41] The estimates of α reported in Table 2 based on the original time series clearly show two distinct clusters: those stations above 60°N (with $a = 1.27$ for FCC and PBQ and α in the interval (0.94,0.98) for ABQ and SOD) and the remaining stations (with α in the interval (1.58, 1.71). This grouping based on the empirical densities of the B_x time series already supports the assertion that the statistical nature of the magnetospheric activities is different for latitudes above 60°N (high latitudes) and those below it (mid- and low latitudes). The high-latitude behavior is consistent with that of the *AE*, which is more strongly influenced by the solar wind, as indicated by the low values of α. On the other hand,

similar values of the exponent α indicate that both mid- and low latitudes have the same statistical nature.

[42] To further examine this latter assertion, we must look at the estimates of the scaling exponent h obtained from a DFA. The last column of Table 1 shows that the exponent h is similar for all the stations. This may be due to the dominance of the local trend component in each time series. This trend component is consistent with the storm pattern apparent in the D_{st}. We have captured this local trend in an empirical mode decomposition. Note that in this EMD approach, there is no need to select a wavelet-type function for the decomposition, and a smooth trend component is obtained after a reasonable number of steps (four intrinisc mode functions as exemplified in Figure 4). After removing this trend component, another DFA is performed on the detrended data; the results are shown in Table 2. It is interesting that the new estimates of the scaling exponent h now show two clear clusters: one consisting of NA1, CEUR, AUS, and ASIA with $h = 1$ approximately, and the other consisting of NA2 and NEUR with $h = 0.75$ approximately. This grouping again confirms that the mid- and low-latitude stations have the same scaling behavior, whereas those in NA2 and NEUR are more strongly influenced by the solar wind. The estimates of the α-stability exponent mostly remain the same for NA1, CEUR, AUS, and ASIA, as well as FCC and PBQ in NA2 and ABK and SOD in NEUR. Those stations STJ and OTT in NA2 and LOV and NUR in NEUR are slightly affected by the detrending. The results indicate that trend removal would not alter in any significant way the clustering obtained in phase 1 above.

[43] Another purpose of this paper is to construct a stochastic model for the detrended (stationary) component of the B_x time series. The model suggested is the FSDE (1). The shape of the empirical density and the estimates of the parameters in Table 2 suggest the use of an α-stable noise to drive the equation. The estimates $h = 1$ then yield the Stokes-Boussinesq-Basset equation (3) for the mid- and low-latitude stations. As noted by *Anh et al.* [2008] in describing the motion of a spherical particle of mass m and radius a in a fluid with kinematic viscosity ν, *Stokes* [1850], *Boussinesq* [1885], and *Basset* [1888] proposed a retarded viscous force given by

$$F(t) = -\frac{1}{\mu} \frac{a}{\sqrt{\pi\nu}} \int_0^t \frac{1}{\sqrt{t-\tau}} \frac{d\xi}{d\tau} d\tau,$$

where $\xi(t)$ is the velocity of the particle and μ denotes the mobility coefficient. On the basis of Newton's second law that force = mass × acceleration, the equation of motion of the particle is described by

$$m\frac{d\xi}{dt} = -\frac{1}{\mu} \frac{a}{\sqrt{\pi\nu}} \int_0^t \frac{1}{\sqrt{t-\tau}} \frac{d\xi}{d\tau} d\tau + \frac{dL}{dt}, \qquad (10)$$

where $\frac{dL}{dt}$ denotes a random force arising from rapid thermal fluctuations. Using the notation of fractional derivative (2) with $n = 1$, equation (10) is identical to equation (3) with suitably defined κ and η. The goodness of fit of the probability densities and realistic simulations from the model indicate that the mid- and low latitudes have the type of

dynamics and scaling as described by the Stokes-Boussinesq-Basset equation (3).

5. Conclusions

[44] The numerical results from DFA show that the B_x time series are nonstationary and antipersistent. The α-stable density fits their empirical densities very well. The time series have pronounced local trends. EMD is found to be a suitable technique to fit the local trends of B_x data. These local trends must be removed before an FSDE can be developed. It is also found that FSDE in combination with EMD simulate very well the B_x time series.

[45] Another finding of this paper is the presence of two distinct scaling behaviors, one in the mid- and low latitudes similar to that of the D_{st} index and the other above latitude 60°N consistent with that of the AE index. These scaling behaviors, as depicted by the α-stability exponent and the scaling exponent, are characteristic of the two clusters of the INTERMAGNET. They map into the inner magnetosphere and the outer magnetosphere, respectively.

[46] The results provide strong evidence that the statistical nature of magnetospheric activities, driven by the solar wind, is different from high latitudes to mid- and low latitudes. The dynamical properties of the magnetosphere are less complex at mid- and low latitudes and can thus be described by fewer degrees of freedom than the high-latitude magnetosphere.

References

Anh, V. V., K. S. Lau, and Z. G. Yu (2002a), Recognition of an organism from fragments of its complete genome, *Phys. Rev. E, 66*, 031910.
Anh, V. V., C. C. Heyde, and N. N. Leonenko (2002b), Dynamic models of long-memory processes driven by Lévy noise, *J. Appl. Probab., 39*, 730–747.
Anh, V. V., and R. McVinish (2003), Fractional differential equations driven by Lévy noise, *J. Appl. Math. Stochastic Anal., 16*, 97–119.
Anh, V. V., J. M. Yong, and Z. G. Yu (2008), Stochastic modeling of the auroral electrojet index, *J. Geophys. Res., 113*, A10215, doi:10.1029/2007JA012851.
Anh, V. V., Z. G. Yu, and J. A. Wanliss (2007), Analysis of global geomagnetic variability, *Nonlin. Proc. Geophys., 14*, 701–708.
Anh, V. V., Z. G. Yu, J. A. Wanliss, and S. M. Watson (2005), Prediction of magnetic storm events using the D_{st} index, *Nonlin. Proc. Geophys., 12*, 799–806.
Basset, A. B. (1888), *A Treatise on Hydrodynamics*, 2, Deighton Bell, Cambridge, U.K.
Boussinesq, J. (1885), Sur la résistence qu'oppose un liquid indé fini en repos, san pesanteur, au mouvement varié d'une sphère solide qu'il mouille sur toute sa surface, quand les faibles pour que leurs carr és et produits soient négligeables, *C. R. Acad. Paris, 100*, 935–937.
Burlaga, L. F. (1991), Multifractal structure of the interplanetary magnetic field: Voyager 2 observations near 25 AU, 1987–1988, *Geophys. Res. Lett., 18*(1), 69–72, doi:10.1029/90GL02596.
Burlaga, L. F. (2001), Lognormal and multifractal distributions of the heliospheric magnetic field, *J. Geophys. Res., 106*, 15,917–15,927, doi:10.1029/2000JA000107.

Burlaga, L. F., C. Wang, and N. F. Ness (2003), A model and observations of the multifractal spectrum of the heliospheric magnetic field strength fluctuations near 40 AU, *Geophys. Res. Lett., 30*(10), 1543, doi:10.1029/2003GL016903.
Cersosimo, D. O., and J. A. Wanliss (2007), Initial studies of high latitude magnetic field data during different magnetospheric conditions, *Earth Planets Space, 59*(1), 39–43.
Chambers, J. M., C. L. Mallows, and B. W. Stuck (1976), A method for simulating stable random variables, *J. Am. Stat. Assoc., 71*, 340–344.
Chang, T. S. (1999), Self-organized criticality, multi-fractal spectra, sporadic localized reconnections and intermittent turbulence in the magnetotail, *Phys. Plasmas, 6*, 4137–4145.
Chapman, S. C., N. W. Watkins, R. O. Dendy, P. Helander, and G. Rowlands (1998), A simple avalanche model as an analogue for magnetospheric activity, *Geophys. Res. Lett., 25*, 2397–2400, doi:10.1029/98GL51700.
Consolini, G., M. F. Marcucci, and M. Candidi (1996), Multifractal structure of auroral electrojet index data, *Phys. Rev. Lett., 76*, 4082–4085.
Freeman, M. P., and N. W. Watkins (2002), The heavens in a pile of sand, *Science, 298*, 979–980.
Huang, N., Z. Shen, S. R. Long, M. L. Wu, H. H. Shih, Q. Zheng, N. C. Yen, C. C. Tung, and H. H. Liu (1998), The empirical mode decomposition and Hilbert spectrum for nonlinear and nonstationary time series analysis. *Proc. R. Soc. London A, 454*, 903–995.
Jaffard, S. (1999), The multifractal nature of Lévy processes, *Probab. Theory Related Fields, 114*, 207–227.
Janosi, I. M., and R. Muller (2005), Empirical mode decomposition and correlation properties of long daily ozone records, *Phys. Rev. E, 71*, 056126.
Kabin, K., and V. O. Papitashvili (1998), Fractal properties of the IMF and the Earths magnetotail field, *Earth Planets Space, 50*, 87–90.
Kantelhardt, J. W., S. A. Zschiegner, E. Koscielny-Bunde, A. Bunde, S. Havlin, and H. E. Stanley (2002), Multifractal detrended fluctuation analysis of nonstationary time series, *Physica A, 316*, 87–114.
Klimas, A. J., V. M. Uritsky, D. Vassiliadis, and D. N. Baker (2004), Reconnection and scale-free avalanching in a driven current-sheet model, *J. Geophys. Res. 109*, A02218, doi:10.1029/2003JA010036.
Lagarias, J. C., J. A. Reeds, M. H. Wright, and P. E. Wright (1998), Convergence properties of the Nelder-Mead simplex method in low dimensions, *SIAM J. Optimization, 9*, 112–147.
Lin, L., Y. Wang, and H. Zhou (2009), Iterative filtering as an alternative for empirical mode decomposition, *Adv. Adaptive Data Anal., 1*(4), 543–560.
Lui, A. T. Y. (2002), Multiscale phenomena in the near-Earth magnetosphere, *J. Atmos. Sol.-Terr. Phys., 64*, 125–143.
Lui, A. T. Y., S. C. Chapman, K. Liou, P. T. Newell, C. I. Meng, M. Brittnacher, and G. K. Parks (2000), Is the dynamic magnetosphere an avalanching system?, *Geophys. Res. Lett., 27*, 911–914, doi:10.1029/1999GL010752.
Lui, A. T. Y., W. W. Lai, K. Liou, and C. I. Meng (2003), A new technique for short-term forecast of auroral activity, *Geophys. Res. Lett., 30*(5), 1258, doi:10.1029/2002GL016505.
Movahed, M. S., G. R. Jafari, F. Ghasemi, S. Rahvar, and M. R. R. Tabar (2006), Multifractal detrended fluctuation analysis of sunspot time series, *J. Stat. Mech.: Theory Exper., 2*, P02003, doi:10.1088/1742-5468/2006/02/P02003.
Mueller, C. (1998), The heat equation with Lévy noise, *Stoch. Proc. Appl., 74*, 67–82.
Nikias, C. L., and M. Shao (1995), *Signal processing with alpha-stable distributions and applications*, John Wiley & Sons, New York.
Nolan, J. P. (2009), *Stable Distributions: Models for Heavy Tailed Data*, Birkhäuser, Boston. In press, Chapter 1 online at academic2.american.edu/~jpnolan.
Peng, C.-K., S. V. Buldyrev, S. Havlin, M. Simons, H. E. Stanley, and A. L. Goldberger (1994), Mosaic organization of DNA nucleotides, *Phys. Rev. E, 49*, 1685–1689.
Podlubny, I. (1999), *Fractional Differential Equations*, Academic Press, San Diego, CA.
Pulkkinen, A., A. Klimas, D. Vassiliadis, and V. Uritsky (2006), Role of stochastic fluctuations in the magnetosphe-ionosphere system: A stochastic model for the AE index variations, *J. Geophys. Res., 111*, A10218, doi:10.1029/2006JA011661.
Pulkkinen, A., A. Klimas, D. Vassiliadis, V. Uritsky, and E. Tanskanen (2005), Spatiotemporal scaling properties of the gound geomegnetic field variations, *J. Geophys. Res., 111*, A03305, doi:10.1029/2005JA011294.
Shi, F., Q. J. Chen, and N. N. Li (2008), Hilbert Huang transform for predicting proteins subcellular location, *J. Biomed. Sci. Eng., 1*, 59–63.
Stokes, G. G. (1850), Mathematical and physical papers, *Trans. Camb. Phil. Soc., 9*.

Uritsky, V. M., A. J. Klimas, D. Vassiliadis, D. Chua, and G. Parks (2002), Scale-free statistics of spatiotemporal auroral emissions as depicted by POLAR UVI images: Dynamic magnetosphere is an avalanching system, *J. Geophys. Res.*, *107*(A12), 1426, doi:10.1029/2001JA000281.

Uritsky, V. M., and M. I. Pudovkin (1998), Low frequency1/*f*-like fluctuations of the AE index as a possible manifestation of self-organized criticality in the magnetosphere, *Ann. Geophys.*, *16*, 1580–1588.

Wanliss, J. A. (2004), Nonlinear variability of SYM-H over two solar cycles, *Earth Planets Space*, *56*, e13–16.

Wanliss, J. A. (2005), Fractal properties of SYM-H during quiet and active times, *J. Geophys. Res.*, *110*, A03202, doi:10.1029/2004JA010544.

Wanliss, J. A., V. V. Anh, Z. G. Yu, and S. Watson (2005), Multifractal modelling of magnetic storms via symbolic dynamics analysis, *J. Geophys. Res.*, *110*, A08214, doi:10.1029/2004JA010996.

Wanliss, J. A., and P. Dobias (2007), Space Storm as a Phase Transition, *J. Atmos. Sol. Terr. Phys.*, *69*, 675–684, doi:10.1016/j.jastp.2007.01.001.

Wanliss, J. A., and M. A. Reynolds (2003), Measurement of the stochasticity of low-latitude geomagnetic temporal variations, *Ann. Geophys.*, *21*, 2025–2030.

Watkins, N. W., D. Credgington, B. Hnat, S. C. Chapman, M. Freeman, and J. Greenhough (2005), Towards synthesis of solar wind and geomagnetic scaling exponents: a fractional Lévy motion model, *Space Sci. Rev.*, *121*, 271–284.

Yu, Z. G., V. Anh, and K. S. Lau (2001a), Measure representation and multifractal analysis of complete genome, *Phys. Rev. E*, *64*, 31903.

Yu, Z. G., V. V. Anh, K. S. Lau, and L. Q. Zhou (2006), Fractal and multifractal analysis of hydrophobic free energies and solvent accessibilities in proteins, *Phys. Rev. E*, *63*, 031920.

Yu, Z. G., V. Anh, and R. Eastes (2009), Multifractal analysis of geomagnetic storm and solar flare indices and their class dependence, *J. Geophys. Res.*, *114*, A05214, doi:10.1029/2008JA013854.

Yu, Z. G., V. Anh, and B. Wang (2001b), Correlation property of length sequences based on global structure of complete genome, *Phys. Rev. E*, *63*, 011903.

Yu, Z. G., V. V. Anh, J. A. Wanliss, and S. M. Watson (2007), Chaos game representation of the Dst index and prediction of geomagnetic storm events, *Chaos, Solitons and Fractals*, *31*, 736–746.

V. Anh and Z.-G. Yu, Discipline of Mathematical Science, Faculty of Science and Technology, Queensland University of Technology, GPO Box 2434, Brisbane, Q4001, Australia. (yuzg1970@yahoo.com)

D. Mao and Y. Wang, Department of Mathematics, Michigan State University, East Lansing, MI 48824-1027, USA.

J. Wanliss, Presbyterian College, 503 South Broad Street, Clinton, SC 29325, USA.